Distributed dynamic event-triggered time-varying resource management for microgrids via practical predefined-time multiagent methods

Tingting Zhou, Salah Laghrouche, Youcef Ait-Amirat

***Abstract*—This paper investigates the problem of time-varying (TV) resource management in microgrids (MGs) under TV demand, employing a multi-agent system (MAS) approach. A novel TV resource management model is introduced, explicitly accounting for dynamic constraints and demand variations to ensure real-time resource allocation while effectively handling load fluctuations and renewable energy variability. To address this problem, a fully distributed predefined-time (PDT) optimization algorithm is developed, incorporating a time-base generator (TBG) to guarantee convergence within a PDT, independently of initial conditions and system parameters. Additionally, a novel dynamic event-triggered (DET) communication mechanism is designed to reduce unnecessary data exchange and ensure scalability under limited communication resources. The effectiveness of the proposed approach is assessed through extensive simulations, which confirm its ability to achieve robust operation, fast convergence, reduced communication overhead, and adaptability to structural changes in the MG, including plug-and-play functionality.**

***Index Terms*—Distributed optimization for time-varying microgrids, Time-varying demand, Dynamic event-triggered mechanism, Predefined-time optimization in multi-agent microgrids.**

Nomenclature

$\varrho(t)$	Binary variable (1: grid-connected, 0: islanded)
$P_i(t)$	Power output of agent i (kW)
$P_{C,i}, P_{R,i}, P_{E,i}$	Power outputs of CDG, REG, ESS i (kW)
$P_{DL,i}, P_{NDL,i}$	Power consumption of DL and NDL i (kW)
P_{grid}	Net power exchange with main grid (kW)
P_x^+, P_x^-	Positive/negative part of P_x (kW)
$P_i^{\max}, P_i^{\min}$	Upper and lower power bounds of agent i (kW)
$\delta_i(t), \eta_i(t), \vartheta_i(t)$	TV cost coefficients ($/kW^{2}h, $/kWh, $/h)
$\lambda_R(t)$	Renewable generation benefit ($/kWh)
$C_{om}(t)$	Operation and maintenance cost ($/kWh)
$\gamma_{\text{cu}}(t)$	Curtailment penalty coefficient ($/kWh)
$P_{R,i}^{\text{av}}(t)$	Forecasted available power of REG i (kW)
$\lambda_E(t)$	Environmental benefit of ESS operation ($/kWh)
$\eta_{\text{ch}}(t), \eta_{\text{di}}(t)$	Charging/discharging efficiency of ESS
$\lambda_{\text{re}}(t)$	Reserve value coefficient (based on SOC)
$c_{\text{cycle}}(t)$	Battery degradation-related cycling cost ($/kWh)
c_{de}	SOC tracking penalty coefficient ($/h)
C_{om}^E	Operation and maintenance cost coefficient ($/kWh)
SOC_{ref}	Reference SOC
$c_{\text{cy}}(t)$	DL degradation cost ($/kWh)
$P_{NDL,i}^{\text{ref}}$	Reference power for NDL i (kW)
$p_{\text{in}}(t), p_{\text{bu}}(t)$	Internal and grid electricity prices ($/kWh)
p_{carbon}	Carbon tax price ($/ton$CO_2$)
$E_{C,i}$	Carbon emissions of CDG i (tonCO_2/h)
$P_{\text{buy}}^{\max}, P_{\text{sell}}^{\max}$	Grid exchange limits (kW)
$W_{C,i}, W_{R,i}, W_{E,i}$	SWFs for CDG, REG, ESS ($/h)
$W_{\text{DL},i}, W_{\text{NDL},i}$	SWFs for DL and NDL ($/h)
W_{grid}	SWF of main grid interaction ($/h)

Abbreviations

TV	Time-Varying
MG	Microgrid
SET	Static Event-Triggered
DET	Dynamic Event-Triggered
SWF	Social Welfare Function
PDT	Predefined-Time
MAS	Multi-Agent System
DER	Distributed Energy Resource
REG	Renewable Energy Generator
ESS	Energy Storage System
SOC	State of Charge
NDL	Non-Dispatchable Load
DL	Dispatchable Load
TBG	Time Base Generator
PnP	Plug-and-Play
FT	Finite-Time
FXT	Fixed-Time
RMP	Resource Management Problem

Tingting zhou, Salah Laghrouche and Youcef Ait-Amirat are with the Department of FEMTO-ST Institute (UMR 6174), CNRS, UTBM, Université Marie et Louis Pasteur, Belfort, F-90000,France (e-mail: tingting.zhou@utbm.fr, salah.laghrouche@utbm.fr and youcef.ait-amirat@univ-fcomte.fr).

I. Introduction

In contemporary grid management, MGs have garnered significant attention due to their flexibility and sustainability. As a crucial component of the electrical grid, MGs are capable of operating independently in the event of power outages or other grid failures [1]. However, effective resource management, especially in scenarios involving renewable energy sources, remains a major challenge. Traditional centralized control methods, though widely adopted, exhibit notable limitations in handling dynamic changes, real-time responsiveness, and system robustness [2].

To address these limitations, scholars have introduced MAS

into MG management, significantly enhancing the system's capabilities for distributed decision-making and autonomous regulation. One of the key advantages of MAS in MG resource management lies in its ability to model the MG as a collection of autonomous agents, each managing specific components such as distributed generators, energy storage units, and loads. These agents coordinate their actions through local communication to optimize resource use and improve energy distribution efficiency [3, 4].

In recent years, the study of RMP has garnered substantial interest among researchers due to its critical role in optimizing operations across various industries. Scholars have extensively explored various aspects of RMP, developing strategies and models to enhance efficiency and reduce costs [5–7]. Traditional RMP formulations often assume static objective functions and constraints. However, in practice, resource availability, demand, and operational constraints vary dynamically over time [8, 9]. To better capture these variations, TV cost functions and dynamic constraints have been introduced, allowing models to more accurately reflect renewable energy fluctuations, price volatility, shifting operational costs, and demand-side responses [10, 11]. For example, in [9], Huang et al. investigated the TV economic dispatch by using a prediction-correction method. The distributed continuous-time algorithms were proposed to solve the RMP with TV quadratic cost functions.

In MG RMP within cyber-physical systems, optimizing communication resources is crucial due to limited bandwidth. Event-triggered communication strategies have been shown to be more efficient than traditional continuous strategies, as they significantly reduce the need for constant data exchange and bandwidth usage [12, 13]. Unlike static event-triggered (SET) methods [14–17] that rely on fixed triggering conditions regardless of system context, DET strategies adapt their triggering rules based on real-time data, thereby offering more robust performance in managing the complex dynamics of MGs. DET mechanisms can respond more flexibly to changes in system states or external conditions, enabling communication only when performance deviates from predefined thresholds or when significant events occur [18–22]. In [19], a DET fixed-time (FXT) distributed strategy was presented for RMP. A novel DET condition and a TBG distributed predefined-time (PDT) algorithm were designed for RMP in [22]. However, these works [5, 6, 19–22] have only focused on time-invariant resource management issues. Therefore, using a fully distributed DET mechanism to solve RMP with TV cost functions and constraints remains a challenging issue.

The rate of convergence is a critical aspect of algorithm performance, particularly in applications such as MG systems, where rapid adjustments are essential due to the inherent variability of renewable energy sources. In recent years, various distributed optimization algorithms have been developed with different convergence properties, including asymptotic [6, 23, 24], finite-time (FT) [25–29], and FXT [30–34] convergence. However, asymptotic convergence algorithms lack explicit bounds on settling time, and the convergence times of FT and FXT algorithms typically depend on the system's initial conditions and parameters. These limitations hinder their applicability in time-sensitive scenarios. To address this issue, the PDT optimization approach has been introduced for solving RMPs [35]. Specifically, the TBG-based PDT algorithm constructs a strongly time-dependent gain function that compresses the system state convergence process into a finite duration. This directly couples the convergence time with physical time. Consequently, users neither need to consider the influence of initial conditions nor manually tune parameters to guarantee system convergence within the PDT. This ensures timely and predictable system responses, which is essential for maintaining stability in highly dynamic environments.

Despite the advancements made in the cited papers, several unresolved challenges persist and require further investigation. For instance, [9–11] addressed TV cost functions but neglects the TV constraints, and it also overlooks significant communication overhead caused by continuous communication demands. Similarly, although some works have explored DET strategies, [12, 13] use asymptotic convergence without explicit settling time bounds. [18] adopts exponential convergence, and [20, 21] rely on linear convergence, both of which lead to slow convergence near equilibrium. These convergence properties limit the responsiveness of the system and may increase operational costs under dynamic and time-sensitive conditions. The works in [25–27, 30–32, 35] focus on improving convergence speed but do not consider the TV characteristics inherent in real-world RMPs in MGs. Notably, to date, few studies have explored TV RMP in MGs under a fully distributed DET-based PDT optimization framework leveraging MASs. Indeed, such research could significantly enhance the efficiency and adaptability of MG operations by reducing communication overhead, accelerating convergence, and enhancing the ability to manage the dynamic integration of renewable energy sources [36, 37].

To address the aforementioned limitations, this paper investigates the time-varying TV RMP in MGs using a MAS framework. We propose a fully distributed DET-PDT optimization algorithm to effectively manage the challenges arising from dynamic system characteristics, limited communication resources, and renewable energy variability. This approach differs substantially from existing studies on RMPs. The main contributions of this work are summarized as follows:

1) A novel distributed practical DET-PDT optimization algorithm is developed. Compared with existing methods for RMPs [5, 6, 6, 8–11, 19–21, 23–27, 32, 35], the proposed algorithm simultaneously achieves PDT convergence, reduced communication overhead, and enhanced scalability.

2) A new DET mechanism is designed, which differs from [12, 13, 18–21], by incorporating a TBG-based with TV gain. This mechanism significantly reduces unnecessary transmissions, ensures fast convergence within PDT, and avoids Zeno behavior.

3) This paper focuses on TV RMP with TV equality constraints. Unlike conventional static resource management [5, 6, 6, 19–22, 24–27, 32, 35], the proposed model better captures the dynamic nature of renewable energy sources in MGs, enabling real-time resource allocation adjustments aligned with practical operational demands.

The remainder of this paper is organized as follows. Sec-

tion II presents the necessary preliminaries on graph theory, basic definitions, and lemmas, as well as an overview of the MAS framework. Section III introduces the modeling of the TV RMP. The proposed distributed DET-PDT optimization algorithm is described in detail in Section IV. Section V provides simulation results. Finally, Section VI concludes the paper.

Notation: Throughout this paper, let $\mathbb{R}$, $\mathbb{R}^N$, and $\mathbb{R}^{N\times M}$ denote the set of real numbers, the N-dimensional real vector space, and the set of $N \times M$ real matrices, respectively. Let $\mathbf{1}_N \in \mathbb{R}^N$ denote the vector with all entries equal to 1. $\mathrm{diag}\{\cdot\}$ denotes a diagonal matrix. For a given vector $x \in \mathbb{R}^N$, the Euclidean norm is defined as $\|x\| = \sqrt{x^\top x}$.

TABLE I
FEATURE COMPARISONS BETWEEN THE DESIGNED ALGORITHM AND EXISTING RESULTS

Ref.	TV objective function	DET	Convergence Type	TV demand	Initialization free
[8]	✓	×	Asymptotic	✓	×
[10]	✓	×	FT	×	×
[11]	✓	×	FT	✓	×
[19]	×	✓	FXT	×	×
[21]	×	✓	Exponential	×	×
[22]	×	✓	PDT	×	✓
[35]	×	×	PDT	×	✓
Herein	✓	✓	PDT	✓	✓

II. PRELIMINARIES

A. Graph Theory

Let $G = (\mathcal{V}, E, A)$ be an undirected graph with N nodes, where $\mathcal{V}$ is the set of nodes, and $E \subset \mathcal{V} \times \mathcal{V}$ denotes the set of edges. The connectivity between the nodes is described by the adjacency matrix $A = [a_{ij}] \in \mathbb{R}^{N\times N}$, where $a_{ij} = 1$ if there exists an edge between nodes i and j, and $a_{ij} = 0$ otherwise. Since the graph is undirected, A is symmetric, i.e., $a_{ij} = a_{ji}$. The neighbor set of node i is defined as $N_i = \{j \in \mathcal{V} : (i,j) \in E\}$. The Laplacian matrix $L = [l_{ij}] \in \mathbb{R}^{N\times N}$ of the graph is defined by $l_{ij} = -a_{ij}$ for $i \neq j$, and $l_{ii} = \sum_{j=1}^{N} a_{ij}$. If the graph is connected, the eigenvalues of L satisfy $0 = \lambda_1(L) < \lambda_2(L) \leq \cdots \leq \lambda_N(L)$. Moreover, L admits the spectral decomposition $L = D^\top H D$, where D is an orthogonal matrix and $H = \mathrm{diag}\{0, \lambda_2(L), \ldots, \lambda_N(L)\}$.

B. TBG-Based PDT Convergence

Consider the following scalar dynamic system:

$$\dot{y}(t) = -\xi T(t, t_m)\, y(t), \quad y(0) > 0, \tag{1}$$

where $y : \mathbb{R} \to \mathbb{R}$, $\xi > 0$, t_m is the predefined convergence time, and $T(t, t_m) : \mathbb{R}_{\geq 0} \times \mathbb{R}^+ \to \mathbb{R}$ is a TBG function, as introduced in [38]. Specifically, the TBG is defined as:

$$T(t, t_m) = d\zeta(t, \tau)/dt, \tag{2}$$

where $\zeta(t, \tau)$ satisfies the following conditions:

(1) $0 < \tau \ll 1$,
(2) $\lim_{\tau\to 0^+}[\zeta(t_m^+, \tau) - \zeta(0, \tau)] = +\infty$,
(3) $\zeta(t, \tau) - \zeta(t_m^+, \tau) \geq 0$ for all $t > t_m$,
(4) $\lim_{t\to+\infty}[\zeta(t, \tau) - \zeta(0, \tau)] = +\infty$.

In this paper, the choice of $T(t, t_m)$ follows the formulation proposed in [39].

Lemma 1 ([38]). *The system* (1)*, with the TBG defined in* (2)*, can achieve practical PDT convergence within* t_m.

Definition 1 ([38]). *A system of the form* $\dot{y}(t) = -\xi T(t, t_m) f(y(t))$*, with* $t \geq 0$*, is said to achieve practical PDT convergence within* t_m *if, for any initial condition* $y(0)$*, there exists* $0 < \nu = \nu(y(0)) \ll 1$ *such that the following conditions hold:*

1) $\lim_{t\to t_m^+} \|y(t)\| \leq \nu$,
2) $\|y(\tilde{t})\| \leq \nu$*, for all* $\tilde{t} \geq t_m$,
3) $\lim_{t\to+\infty} \|y(t)\| = 0$.

C. MAS framework

As shown in Fig. 1, the proposed MAS-based control framework consists of three primary layers: the *Device Layer*, the *Control Layer*, and the *Communication Layer*.

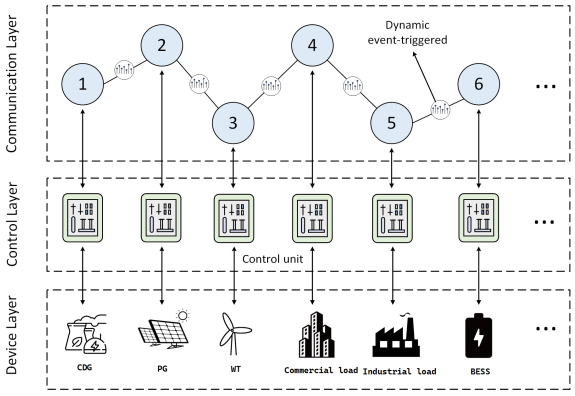

Fig. 1. MAS-Based Three-Layer Structure of a MG with DET Coordination.

The **Device Layer** comprises various components in the MG, including conventional dispatchable generators (CDGs), photovoltaic (PV) systems, wind turbines (WTs), commercial and industrial loads, and energy storage systems (ESSs). These components form the physical infrastructure of the microgrid, responsible for energy generation, storage, and consumption.

The **Control Layer** serves as the intermediary between the physical devices and the communication system. It processes control signals and status updates, ensuring that the power output of the devices aligns with the reference signals provided by the optimization algorithm.

The **Communication Layer** facilitates information exchange among agents. Each agent communicates with its neighbors to share locally computed decisions and updated system states. This layer integrates a DET mechanism, which significantly reduces communication overhead by transmitting updates only when specific conditions, determined by real-time system requirements, are satisfied.

The key to the control process is the calculation of the optimal reference signal generated by the optimization algorithm in the communication layer, which is then transmitted to the

control layer. The control layer adjusts the power output of the device layer to align with the optimal reference signal, thereby achieving optimal system operation and efficient resource utilization.

D. Useful Lemmas

Lemma 2 (Young's Inequality). *For any vectors $a, b \in \mathbb{R}^n$ and any scalar $\epsilon > 0$, the following inequality holds:*

$$a^\top b \leq \frac{\epsilon}{2}\|a\|^2 + \frac{1}{2\epsilon}\|b\|^2.$$

Lemma 3 (Laplacian Spectral Decomposition [22]). *Let $L \in \mathbb{R}^{N\times N}$ be the Laplacian matrix of a connected undirected graph. Then there exists an orthogonal matrix $Q = [q_1\ Q_2] \in \mathbb{R}^{N\times N}$, with $q_1 = \frac{1}{\sqrt{N}}\mathbf{1}_N$, such that*

$$L = Q\begin{bmatrix}0 & 0\\ 0 & J\end{bmatrix}Q^\top,$$

where $J = \mathrm{diag}(\lambda_2, \ldots, \lambda_N)$ contains the nonzero eigenvalues of L.

III. TV RMP Formulation

A. Economic modeling of devices in MGs

To formulate the TV RMP in MGs, we consider the social welfare functions (SWFs) of various components, including CDGs, renewable energy generators (REGs), ESSs, loads, and grid interaction mechanisms. The model is designed to accommodate both islanded and grid-connected MG configurations. To this end, a binary function $\varrho(t) \in \{0, 1\}$ is introduced to indicate the operational mode:

$$\varrho(t) = \begin{cases}0, & \text{islanded mode},\\ 1, & \text{grid-connected mode}.\end{cases} \tag{3}$$

When $\varrho(t) = 1$, the MG is allowed to interact with the main grid; otherwise, it operates in isolation. The value of $\varrho(t)$ is predefined based on the MG's operating mode and remains constant during each optimization process.

1) CDGs: CDGs refer to controllable generation units such as natural gas generators and diesel generators, capable of actively regulating their power output. To better align with practical conditions, the associated generation costs are modeled as a TV quadratic function of active power, expressed as follows [27, 32]:

$$C_{C,i}(P_{C,i}, t) = \delta_{C,i}(t)P_{C,i}^2 + \eta_{C,i}(t)P_{C,i} + \vartheta_{C,i}(t), \quad i \in \mathcal{C}, \tag{4}$$

where $\delta_{C,i}(t)$, $\eta_{C,i}(t)$, and $\vartheta_{C,i}(t)$ are time-varying coefficients representing the nonlinear generation cost, marginal cost, and fixed cost, respectively. The generation output is subject to physical constraints:

$$P_{C,i}^{min} \leq P_{C,i} \leq P_{C,i}^{max}. \tag{5}$$

Where $P_{C,i}^{min}$ and $P_{C,i}^{max}$ are the lower and upper power output limits. Then, the SWF of CDG can be defined as:

$$W_{C,i} = p_{\text{in}}(t)P_{C,i} - C_{C,i} - p_{\text{carbon}}E_{C,i}. \tag{6}$$

Where $p_{\text{in}}(t)$, p_{carbon} and $E_{C,i}$ denote the MG internal electricity price, carbon tax price and carbon emissions intensity, respectively.

2) REGs: For REGs such as PV and WT units, the SWF accounts for environmental benefits, electricity sales revenue, curtailment penalties, and operational costs. Specifically, inspired by the modeling approaches in [40], the welfare of agent $i \in \mathcal{R}$ is defined as:

$$\begin{aligned} W_{R,i}(t) &= \big(\lambda_R(t) + p_{\text{in}}(t) - C_{\text{om}}(t)\big)P_{R,i} - C_{R,i}(t),\\ C_{R,i}(t) &= \eta_{R,i}(t)P_{R,i} + \delta_{R,i}(t)\exp\big(\gamma_{\text{cu}}(t)(P_{R,i}^{\text{av}} - P_{R,i})\big),\end{aligned} \tag{7}$$

subject to:

$$0 \leq P_{R,i} \leq P_{R,i}^{\text{av}}. \tag{8}$$

Here, $\lambda_R(t)$ denotes the per-unit environmental value of renewable energy, $C_{\text{om}}(t)$ is the operation and maintenance cost per unit of electricity, $\eta_{R,i}(t)$ and $\delta_{R,i}(t)$ are TV nonnegative cost coefficients; $\gamma_{\text{cu}}(t)$ is the curtailment penalty coefficient, and $P_{R,i}^{\text{av}}(t)$ is the forecasted maximum available renewable output.

3) ESSs: Dynamic modeling of ESSs plays a vital role in improving system-level economy and reliability. This paper presents a TV optimization framework for ESSs that jointly considers energy arbitrage, environmental benefits, and degradation costs. The model integrates key operational constraints such as charging/discharging efficiency, state of charge (SOC), and power exchange limits. It also supports both grid-connected and islanded modes by dynamically adjusting grid interaction strategies, enhancing system resilience to price fluctuations and external disturbances. The SWF of ESS agent $i \in \mathcal{E}$ is defined as:

$$W_{E,i} = B_{\text{ar},i} + B_{\text{en},i} + B_{\text{ba},i} - C_{\text{lo},i} - C_{\text{ma},i}, \tag{9}$$

where each term represents the following components: $B_{\text{ar},i}(t)$: Arbitrage benefit; $B_{\text{en},i}(t)$: Environmental benefit; $B_{\text{ba},i}(t)$: Backup capacity value; $C_{\text{lo},i}(t)$: Loss and degradation cost; $C_{\text{ma},i}(t)$: Operation and maintenance cost. These components are defined as follows:

$$B_{\text{ar},i}(t) = \varrho(t)\left(p_{\text{in}}(t)P_{i,E}^{+} - p_{\text{bu}}(t)(P_{i,E}^{-})\right), \tag{10}$$

$$B_{\text{en},i}(t) = \lambda_E(t)\left(\eta_{\text{ch}}(t)(P_{i,E}^{-}) - (1/\eta_{\text{di}}(t))P_{i,E}^{+}\right), \tag{11}$$

$$B_{\text{ba},i}(t) = \lambda_{\text{re}}(t)\cdot \text{SOC}(t), \tag{12}$$

where $P_{i,E}^{+} = \frac{1}{2}(P_{i,E}(t) + \sqrt{P_{i,E}^2(t) + \epsilon})$ and $P_{i,E}^{-} = \frac{1}{2}(P_{i,E}(t) + \sqrt{P_{i,E}^2(t) + \epsilon})$ represent the discharge and charge power of ESS i, respectively, with ϵ being a small constant. The exchanged power is bounded by:

$$-P_{i,E}^{\max} \leq P_{i,E} \leq P_{i,E}^{\max}. \tag{13}$$

Here, $p_{\text{bu}}(t)$ denote the external electricity prices, respectively. $\lambda_E(t)$ represents the equivalent environmental benefit per unit of stored energy, while $\eta_{\text{ch}}(t)$ and $\eta_{\text{di}}(t)$ denote the charging and discharging efficiencies. $\lambda_{\text{re}}(t)$ captures the reserve value associated with the SOC level.

The cost terms are given by [41, 42]:

$$C_{\text{lo},i}(t) = c_{\text{cycle}}(t)\sqrt{P_{i,E}^2 + \epsilon} + c_{\text{de}}\left(\text{SOC}(t) - \text{SOC}_{\text{ref}}\right)^2, \tag{14}$$

$$C_{\text{ma},i}(t) = C_{\text{om}}^{E}P_{i,E}^2, \tag{15}$$

where degradation cost $C_{\text{lo},i}(t)$ is a simplified approximation that considers only the primary effects of cycle-related degradation and SoC deviation. $c_{\text{cycle}}(t)$ reflects degradation-related cycling loss, $\sqrt{P_{i,E}^2+\epsilon}$ is used as a smooth approximation of the absolute value function and c_{de} is a penalty coefficient that encourages SOC tracking to prolong battery life. SOC_{ref} denotes a reference SOC target for long-term health optimization. The parameter C_{om}^{E} represents the unit operational and maintenance cost during charging or discharging.

4) Load Devices: To accurately capture the impact of different load types on system performance, this paper distinguishes between dispatchable loads (DLs) and non-dispatchable loads (NDLs), and develops corresponding SWFs for each category.

1) DLs: For DLs, the SWF is modeled as a TV function of active power consumption, incorporating economic benefits, diminishing marginal utility, electricity cost, and degradation effects. Specifically, motivated by the formulation in [42], the SWF of agent $i \in \mathcal{D}$ is given by:

$$\begin{aligned} W_{\text{DL},i} &= \eta_{\text{DL},i}(t)P_{\text{DL},i} - \delta_{\text{DL},i}(t)P_{\text{DL},i}^2 - C_{\text{DL},i}(t), \\ C_{\text{DL},i}(t) &= \left(p_{\text{in}}(t) + c_{\text{cy}}(t)\right) P_{\text{DL},i}, \end{aligned} \tag{16}$$

where $P_{\text{DL},i}(t)$ is the power consumed by DL i, subject to:

$$0 \le P_{\text{DL},i} \le P_{\text{DL},i}^{\max}. \tag{17}$$

Here, $\eta_{\text{DL},i}(t)$ denotes the marginal utility of load consumption (e.g., comfort or productivity gain), $\delta_{\text{DL},i}(t)$ represents the marginal utility reduction coefficient, and $c_{\text{cy}}(t)$ captures degradation-related cycling cost.

2) NDLs: NDLs represent critical or inflexible loads that are not subject to real-time optimization. Their SWF formulation prioritizes consumption stability while accounting for energy costs and deviations from a reference profile. For agent $i \in \mathcal{N}$, the SWF is defined as:

$$\begin{aligned} W_{\text{NDL},i}(t) =& \eta_{N,i}(t)\log\left(1+\frac{P_{\text{NDL},i}(t)}{P_{\text{NDL},i}^{\text{ref}}}\right) \\ &- \delta_{N,i}(t)\left(\frac{P_{\text{NDL},i}}{P_{\text{NDL},i}^{\text{ref}}}-1\right)^2 - p_{\text{in}}(t)P_{\text{NDL},i}, \end{aligned} \tag{18}$$

subject to:

$$0 < P_{\text{NDL},i}(t) \le P_{\text{NDL},i}^{\max}. \tag{19}$$

In this model, $\eta_{N,i}(t)$ quantifies the importance of meeting the electricity demand of NDL i at time t, serving as a preference weight in the utility function, $\delta_{N,i}(t)$ penalizes deviations from the preferred consumption level $P_{\text{NDL},i}^{\text{ref}}$, and $p_{\text{in}}(t)$ represents the energy cost.

5) Grid Interaction (GI): The SWF for grid interaction aims to optimize the economic performance of power exchange between the MG and the main grid, while maintaining operational flexibility under different grid conditions. It accounts for both electricity purchase costs and power selling revenues, adjusted dynamically by real-time market prices [42]:

$$W_{\text{grid}}(t) = \varrho(t)\left(p_{\text{in}}(t)\cdot P_{\text{grid}}^{-}(t) - p_{\text{bu}}\cdot P_{\text{grid}}^{+}\right) - \delta_{g,i}(t)P_{\text{grid}}^2(t), \tag{20}$$

where $\delta_{g,i}(t)$ is positive TV correction coefficient, $P_{\text{grid}}(t)$ is the net power exchanged with the grid, constrained by:

$$-\varrho(t)P_{\text{sell}}^{\max} \le P_{\text{grid}}(t) \le \varrho(t)P_{\text{buy}}^{\max}. \tag{21}$$

Here, $P_{\text{grid}}^{+}(t) = \frac{1}{2}\left(P_{\text{grid}}(t) + \sqrt{P_{\text{grid}}^2(t)+\epsilon}\right)$ and $P_{\text{grid}}^{-}(t) = \frac{1}{2}\left(-P_{\text{grid}}(t) + \sqrt{P_{\text{grid}}^2(t)+\epsilon}\right)$ denote the power from and sold to the grid, respectively. $P_{\text{sell}}^{\max}$ and $P_{\text{buy}}^{\max}$ represent the maximum power sale and maximum power purchase, respectively. The formulation (20) captures both the economic incentives associated with real-time electricity trading and the potential operational risks arising from excessive grid interaction.

B. Social welfare maximization model for MG operation

For both islanded and grid-connected modes, the overall SWF of the MG is defined as the aggregate of the individual SWFs of all constituent components, including generation units, storage systems, loads, and grid interaction. Meanwhile, the MG must satisfy a power balance constraint to ensure stable operation, as well as various inequality constraints that reflect physical and operational limitations. Accordingly, the social welfare maximization problem is formulated as follows:

$$\begin{aligned} \max_{\{P_i(t)\}} \quad & \sum_{i\in\mathcal{C}} W_{C,i}(t) + \sum_{i\in\mathcal{R}} W_{R,i}(t) + \sum_{i\in\mathcal{E}} W_{E,i}(t) \\ & + \sum_{i\in\mathcal{D}} W_{\text{DL},i}(t) + \sum_{i\in\mathcal{N}} W_{\text{NDL},i}(t) + W_{\text{grid}}(t) \end{aligned} \tag{22}$$

$$\begin{aligned} \text{s.t.} \quad & (5),(8),(13),(17),(19),(21) \\ & \sum_{i\in\mathcal{C}} P_{C,i}(t) + \sum_{i\in\mathcal{R}} P_{R,i}(t) + \sum_{i\in\mathcal{E}} P_{E,i}(t) + \varrho(t)P_{\text{grid}}(t) \\ & = \sum_{i\in\mathcal{D}} P_{\text{DL},i}(t) + \sum_{i\in\mathcal{N}} P_{\text{NDL},i}(t) \end{aligned}$$

In this study, we investigate an MAS-based RMP for a system comprising the main grid and a MG with N agents. For notational simplicity, we denote $P_i(t)$, $d_i(t)$, and $W_i(P_i(t),t)$ as the output power, demand, and TV SWF of agent i, respectively. The agents include CDGs, REGs, ESSs, DLs, NDLs, and GI. Each agent optimizes its local power dispatch while collectively maintaining system-wide balance. The operational bounds are given by $P_i^{\min} \le P_i(t) \le P_i^{\max}$.

Remark 1. *The proposed model* (22) *captures key dynamic features of MG operation and supports real-time social welfare optimization. It incorporates: (i) TV cost/benefit functions, enabling adaptation to load and renewable fluctuations; (ii) equality constraints for real-time power balance; (iii) inequality constraints ensuring operational feasibility; and (iv) seamless switching between islanded and grid-connected modes. By allowing dynamic adjustment of power and pricing strategies, the model achieves a balance between accuracy and computational efficiency. Its structure also enhances robustness and practical applicability across diverse MG scenarios.*

IV. DET PDT DISTRIBUTED SOLUTION FOR THE RMP

A. Model formulation

Based on this MAS framework, Social welfare maximization problem (22) is reformulated as follows:

$$\begin{aligned} \min \quad & -\sum_{i=1}^{N} W_i(P_i(t),t) \\ \text{s.t.} \quad & \sum_{i=1}^{N} P_i(t) = \sum_{i=1}^{N} d_i(t) \\ & P_i^{min}(t) \le P_i(t) \le P_i^{max}(t), \quad i = 1,...,N. \end{aligned} \tag{23}$$

In this framework, the main grid is treated as an agent when the MG operates in grid-connected mode. In islanded mode, the power output of the main grid agent is set to zero, ensuring autonomous operation of the MG. Additionally, when agent i represents a load (DL/NDL), $d_i(t) > 0$; otherwise, $d_i(t) = 0$.

To address the inequality constraints in (23) and simultaneously ensure that the inequality constraints are strictly satisfied, we utilize the following barrier function technique[43].

$$J_i(P_i(t),t) = \check{W}_i(P_i(t),t) - (1/\varrho_i(t))(\log(\varphi_{i,1}\cdot\varphi_{i,2})), \tag{24}$$

where $\check{W}_i(P_i(t),t) = -W_i(P_i(t),t)$, $\varphi_{i,1} = 1-\varrho_i(t)(P_i(t) - P_i^{max}(t))$ and $\varphi_{i,2} = 1-\varrho_i(t)(P_i^{min}(t) - P_i(t))$. $\varrho(t) \in R$ is chosen as a positive, time-varying function to ensure that it grows unbounded as $t \to \infty$. One possible choice for $\varrho_i(t)$ is the exponential function $\varrho(t) = \epsilon_1 \exp(\epsilon_2 t)$, $\epsilon_1, \epsilon_2 > 0$.

Then, the RMP (23) is reformulated as follows:

$$\begin{aligned} \min \quad & J(P(t),t) = \sum_{i=1}^{N} J_i(P_i(t),t) \\ \text{s.t.} \quad & \sum_{i=1}^{N} P_i(t) = \sum_{i=1}^{N} d_i(t). \end{aligned} \tag{25}$$

Let $\bar{P}^*(t)$ denote the optimal solution to the original problem (23), and $\tilde{P}^*(t)$ denote the optimal solution to the barrier-based problem (25). According to Theorem 1 in [43], if $\varrho_i(t) \to \infty$ as $t \to \infty$, then the solution to the penalized problem asymptotically converges to that of the original problem, i.e.,

$$\lim_{t\to\infty} \|\bar{P}^*(t) - \tilde{P}^*(t)\| = 0.$$

This guarantees that solving the barrier-augmented problem (25) yields an asymptotically optimal solution to the constrained problem (23). For notational simplicity, the dependence on time t is omitted in the subsequent expressions. In addition, we adopt a set of widely used assumptions, consistent with those in the literature (e.g., [43–45]):

Assumption 1 (Slater's Condition): There exists a feasible solution $\{P_i\}_{i=1}^N$ such that the equality constraint $\sum_{i=1}^N P_i = \sum_{i=1}^N d_i$ is satisfied for all $t \ge 0$.

Assumption 2 (Network Connectivity): The agent communication graph G is undirected and connected.

Assumption 3 (Objective Function Regularity): For all $t \ge 0$, each function $J_i(P_i,t)$ is continuously differentiable in both P_i and t, and uniformly c_i-strongly convex in P_i. Moreover, $\frac{\partial}{\partial t}\nabla J_i$ is l_i-Lipschitz with respect to P_i.

Remark 2. *The l_i-Lipschitz condition of $\frac{\partial}{\partial t}\nabla J_i(P_i,t)$ with respect to P_i ensures that the temporal variation of the gradient remains smooth and bounded. This condition helps prevent abrupt changes in the behavior of the objective function caused by time variation. In practice, this assumption is mild and holds for quadratic cost functions with bounded third-order derivatives, as well as other smooth convex functions (e.g., $\alpha(t)\log(1+P_i)$, $\alpha(t)\log(1+e^{P_i})$ and $\alpha(t)e^{P_i}$), provided that $\dot{\alpha}(t)$ is bounded and P_i lies within a compact set.*

B. Distributed Algorithm Design

To solve problem (25), we propose a distributed DET algorithm with PDT convergence. The algorithm ensures reduced communication frequency and independence from initial conditions. The update rules for agent i are given by:

$$\begin{cases} \dot{P}_i(t) = -T(t,t_m)(k_1\nabla_P J_i(P_i,t) + \partial\nabla_P J_i(P_i,t)/\partial t \\ \qquad\qquad - k_1 w_i(t_k^i) - z_i(t_k^i)) \\ \dot{w}_i(t) = -T(t,t_m)(\sum_{j\in N_i} a_{ij}(w_i(t_k^i) - w_j(t_k^j)) \\ \qquad\qquad + \xi_i(t_k^i) - k_2 d_i(t) + k_2 P_i(t_k^i)) \\ \dot{\xi}_i(t) = T(t,t_m)\sum_{j\in N_i} a_{ij}(w_i(t_k^i) - w_j(t_k^j)) \\ \dot{z}_i(t) = T(t,t_m)(\partial\nabla_P J_i(P_i,t)/\partial t - z_i(t_k^i)) \end{cases} \tag{26}$$

Here, w_i, ξ_i, and z_i are auxiliary variables. $J_i(P_i,t)$ and $d_i(t)$ are local variables that can be accessed in real time by agent i. The parameters are selected such that $k_1 > (8m+4\bar{l})/\underline{c}$ and $k_2 = k_1 - 2m$, where $m > 0$, $\bar{l} = \max\{l_i\}_{i=1}^N$, and $\underline{c} = \min\{c_i\}_{i=1}^N$. The initial values satisfy $\mathbf{1}_N^\top \xi_0 = 0$, with $\xi_0 = [\xi_1(0),\ldots,\xi_N(0)]^\top$. The function $T(t,t_m)$ is defined in (2) and ensures PDT convergence via the TBG mechanism. The event-triggered updates occur at discrete time instances $\{t_k^i\}_{k=1}^\infty$, where t_k^j denotes the latest triggering time of agent j. Between two consecutive triggers, i.e., for $t \in [t_k^i, t_{k+1}^i)$, each agent evolves according to the above dynamics.

Remark 3. *In (26), the term $k_1\nabla_P J_i(P_i,t) + \partial\nabla_P J_i(P_i,t)/\partial t - k_1 w_i(t_k^i) - z_i(t_k^i)$ compensates for both spatial and temporal variations in the objective function, ensuring that the system tracks the TV optimal trajectory. The auxiliary variable w_i estimates the aggregated gradient flow and assists in enforcing the global equality constraint in a distributed manner. The term ξ_i ensures consensus among agents on marginal cost information. Finally, z_i compensates for the temporal drift induced by the time variation in $\nabla_P J_i(P_i,t)$.*

Remark 4. *It is worth noting that the initialization condition $\sum_{i=1}^n \xi_i(0) = 0$ is required In (26) to ensure the global equality constraint is satisfied throughout the system's evolution. While the initialization condition exhibits a degree of global dependency, it requires only a one-time coordination at the start of the system and does not involve any centralized computation or global communication during execution. Therefore, the algorithm remains fully distributed during operation, with a coordinated initialization phase.*

To simplify the notation, define $\hat{P}_i(t) = P_i(t_k^i)$, $\hat{w}_i(t) = w_i(t_k^i)$, $\hat{z}_i(t) = z_i(t_k^i)$, $\hat{\xi}_i(t) = \xi_i(t_k^i)$ and $J_i(t) = J_i(P_i,t)$.

Let $e_{Pi}(t) = \hat{P}_i(t) - P_i(t)$, $e_{wi}(t) = \hat{w}_i(t) - w_i(t)$, $e_{zi}(t) = \hat{z}_i(t) - z_i(t)$ and $e_{\xi i}(t) = \hat{\xi}_i(t) - \xi_i(t)$ as the event-triggered state errors. And define the total error as $e_i(t) = e_{P_i}^2 + e_{w_i}^2 + e_{z_i}^2 + e_{\xi_i}^2$. Following this, the DET condition for agent i is constructed as:

$$t_{k+1}^i = \inf\{t : t \geq t_k^i, \gamma_i e_i(t) \geq \theta_i(t)\}, \tag{27}$$

where $\gamma_i > (1-\rho_i)/\tau_i$, and the threshold variable $\theta_i(t)$ evolves as:

$$\theta_i(t) = \exp\left(-\tau_i \int_0^t T(s,t_m)\, ds\right) \times \left(\alpha_i - \rho_i \int_0^t T(s,t_m) e_i(s)\, ds\right) \tag{28}$$

with $\alpha_i > 0$, $\tau_i > 0$, and $\rho_i \in (0,1)$.

Remark 5. *The threshold $\theta_i(t)$ consists of two parts: an exponential decay term and an error-driven integral term. The exponential factor ensures overall threshold reduction over time, while the integral term adapts based on accumulated errors. Large errors accelerate the decay of $\theta_i(t)$, promoting more frequent updates. Conversely, small errors maintain a higher threshold, reducing unnecessary communications. Compared to static or fixed-period triggering, this dynamic design adaptively balances performance and communication efficiency by triggering only when needed.*

Remark 6. *The parameter configuration in Algorithm 1 critically influences convergence performance, communication efficiency, and stability. The pair (k_1, k_2) should be chosen to satisfy $k_1 > (8m + 4\bar{l})/\underline{c}$ and $k_2 = k_1 - 2m$ to determine the PDT convergence behavior. The event-triggering parameters γ_i, τ_i, ρ_i, and α_i collectively regulate the update threshold $\theta_i(t)$, balancing triggering frequency and responsiveness. Additionally, t_m determines the global settling horizon, and ν defines the terminal accuracy band. Proper parameter tuning is essential to ensure stability, Zeno-free behavior, and optimal performance in dynamic MG environments.*

For analytical convenience, the distributed dynamics in (26) can be compactly written as:

$$\begin{cases} \dot{P} = -T(t,t_m)\left(k_1 \nabla_P J + \partial \nabla_P J/\partial t - k_1 \hat{w} - \hat{z}\right), \\ \dot{w} = -T(t,t_m)\left(L\hat{w} + \hat{\xi} - k_2 d + k_2 \hat{P}\right), \\ \dot{z} = T(t,t_m)\left(\partial \nabla_P J/\partial t - \hat{z}\right), \\ \dot{\xi} = T(t,t_m) L\hat{w}, \end{cases} \tag{29}$$

where $P, w, \xi, z, \hat{P}, \hat{w}, \hat{\xi}, \hat{z}, \nabla_P J, d \in \mathbb{R}^N$ are vectors whose ith components correspond to $P_i, w_i, \xi_i, z_i, \hat{P}_i, \hat{w}_i, \hat{\xi}_i, \hat{z}_i$, $\nabla_P J_i$, and d_i, respectively.

Before the convergence analysis, we first establish several fundamental properties of the closed-loop system (29): 1) Optimality of its equilibrium point; 2) Invariance of inequality constraints under the barrier dynamics; 3) Positivity of the internal threshold $\theta_i(t)$ in the event-triggered mechanism. These results form the theoretical basis for the subsequent stability and optimality analysis.

Algorithm 1 Distributed DET PDT Resource Management

Require: Agent set $\mathcal{V}$, parameters $\gamma_i, \tau_i, \rho_i, \alpha_i, k_1, k_2, a_{ij}$, initial states $P(0), w(0), z(0), \xi_0$ with $1_N^T \xi_0 = 0$, TBG function $T(t,t_m)$, horizon T_{end}, convergence threshold ν.

Ensure: Optimal solution P^*, triggering instants $\{t_k^i\}$.

1: **for** $i \in \mathcal{V}$ **do**
2: Configure RMP: $d_i(t), P_i^{\min}(t), P_i^{\max}(t)$
3: Initialize $t_0^i = 0$, $k = 0$, $\hat{P}_i = P_i(0)$, $\hat{w}_i = w_i(0)$, $\hat{z}_i = z_i(0)$, $\hat{\xi}_i = \xi_i(0)$
4: **while** $t \leq T_{\text{end}}$ **do**
5: Update threshold:

$$\theta_i(t) = \exp\left(-\tau_i \int_0^t T(s,t_m)\, ds\right) \times \left(\alpha_i - \rho_i \int_0^t T(s,t_m) e_i(s)\, ds\right)$$

6: **if** $\gamma_i e_i(t) \geq \theta_i(t)$ **then**
7: $t_{k+1}^i \leftarrow t$, broadcast $(\hat{P}_i, \hat{w}_i, \hat{z}_i, \hat{\xi}_i)$
8: Update stored states: $\hat{P}_i \leftarrow P_i(t)$, etc.
9: **end if**
10: Execute control laws:

$$\begin{aligned} \dot{P}_i =& T(t,t_m)(k_1 \nabla_P J_i + \partial \nabla_P J_i/\partial t - k_1 \hat{w}_i - \hat{z}_i) \\ \dot{w}_i =& -T(t,t_m)(\textstyle\sum_{j\in N_i} a_{ij}(\hat{w}_i - \hat{w}_j) + \hat{\xi}_i \\ & - k_2 d_i + k_2 \hat{P}_i) \\ \dot{z}_i =& T(t,t_m)(\partial \nabla_P J_i/\partial t - \hat{z}_i) \\ \dot{\xi}_i =& T(t,t_m) \textstyle\sum_{j\in N_i} a_{ij}(\hat{w}_i - \hat{w}_j) \end{aligned}$$

11: Ensure $t_{k+1}^i - t_k^i \geq \epsilon$ (prevent Zeno)
12: **end while**
13: Verify practical PDT convergence:

$$\lim_{t \to t_m^+} \|P(t) - P^*\| \leq \nu, \quad \|P(\tilde{t}) - P^*\| \leq \nu,\ \forall \tilde{t} > t_m,$$

$$\lim_{t\to\infty} \|P(t) - P^*\| = 0$$

14: **end for**
15: **return** $P^* \leftarrow P(T_{\text{end}})$

Lemma 4 (Optimality of the Equilibrium Point)**.** *Under Assumptions 1–3, for any initial condition $P_i(0) \in \mathcal{D}_i(0)$, $i = 1, \ldots, N$, if (P^*, w^*, ξ^*, z^*) is an equilibrium point of system* (29)*, then P^* is the unique optimal solution of the TV optimization problem* (25)*.*

Proof. Let $J^* := J(P^*, t)$. At equilibrium, all time derivatives vanish, and system (29) reduces to:

$$\begin{cases} 0 = -T(t,t_m)\left(k_1 \nabla_P J^* + \partial \nabla_P J^*/\partial t - k_1 w^* - z^*\right), \\ 0 = -T(t,t_m)\left(Lw^* + \xi^* - k_2 d + k_2 P^*\right), \\ 0 = T(t,t_m)\left(\partial \nabla_P J^*/\partial t - z^*\right), \\ 0 = T(t,t_m) L w^*. \end{cases} \tag{30}$$

From the last two equations in (30), we immediately have

$$z^* = \partial \nabla_P J^*/\partial t, \quad Lw^* = 0 \Rightarrow w_i^* = w_j^*,\ \forall i, j.$$

Thus, w^* reaches consensus.

Next, consider the fourth equation of system (29). Multiplying both sides by $1_N^\top$, we obtain

$$1_N^\top \dot{\xi} = 1_N^\top T(t,t_m) L\hat{w} = 0 \Rightarrow 1_N^\top \xi = \text{const}.$$

Assuming $\mathbf{1}_N^\top \xi(0) = 0$, it follows that $\mathbf{1}_N^\top \xi^* = 0$.

Now summing the second equation of (30) over all agents

$$\mathbf{1}_N^\top (Lw^* + \xi^*) = k_2 \mathbf{1}_N^\top (d - P^*).$$

Since $Lw^* = 0$ and $\mathbf{1}_N^\top \xi^* = 0$, this implies:

$$\sum_{i=1}^{N} P_i^* = \sum_{i=1}^{N} d_i(t).$$

Finally, from the first equilibrium equation and $z^* = \frac{\partial}{\partial t} \nabla_P J^*$, we obtain:

$$\nabla_P J^* = w^*.$$

Therefore, P^* satisfies the KKT conditions of problem (25). Under Assumption 3, the problem is strongly convex, hence P^* is the unique optimal solution. □

The structure of the barrier function in (24) ensures that $J_i(P_i(t), t)$ is well-defined only when the inequality constraints are strictly satisfied. The following result guarantees that if the initial state is feasible, it remains strictly feasible for all time.

Lemma 5 (Invariance of the Feasible Set)**.** *Suppose the initial condition satisfies* $P_i(0) \in \mathcal{D}_i(0) := \{P_i \in \mathbb{R} \mid \varphi_{i,1}(0) > 0,\ \varphi_{i,2}(0) > 0\}$*, where* $\varphi_{i,1}$ *and* $\varphi_{i,2}$ *are as defined in* (24)*. Then, under the controller* (26)*, the state* $P_i(t)$ *remains strictly within the feasible region for all* $t \geq 0$*, i.e.,*

$$P_i^{\min}(t) < P_i(t) < P_i^{\max}(t), \quad \forall t \geq 0.$$

Proof. The barrier term

$$-(1/\varrho(t)) \log(\varphi_{i,1}(t) \cdot \varphi_{i,2}(t))$$

is well-defined only when $\varphi_{i,1}, \varphi_{i,2} > 0$, i.e., when $P_i(t) \in (P_i^{\min}(t), P_i^{\max}(t))$.

Given $P_i(0) \in \mathcal{D}_i(0)$, we consider the gradient behavior near the boundary:

$$\lim_{P_i(t) \to P_i^{\min}(t)^+ \text{ or } P_i^{\max}(t)^-} \nabla_{P_i} J_i(P_i(t), t) = \pm\infty.$$

Thus, the control input $\dot{P}_i(t) \propto -\nabla_{P_i} J_i(P_i(t), t)$ grows unbounded in a direction that pushes the state back into the interior. Therefore, the boundary is repelling and cannot be reached in finite time. Hence, the trajectory remains strictly within the feasible set for all $t \geq 0$. □

Next, we analyze the evolution of the internal threshold variable $\theta_i(t)$ in the DET mechanism and show that it remains strictly positive for all $t \geq 0$.

Lemma 6 (Positivity of the Threshold Variable)**.** *The dynamic threshold variable* $\theta_i(t)$ *defined in* (28) *remains strictly positive for all* $t \geq 0$*.*

Proof. From the definition of $\theta_i(t)$, we have:

$$\dot{\theta}_i(t) = T(t, t_m) \left(-\tau_i \theta_i(t) - \rho_i e_i(t)\right),$$

with initial condition $\theta_i(0) = \alpha_i > 0$.

Under the DET condition (27), during non-triggering intervals we have $\gamma_i e_i(t) < \theta_i(t)$, which implies:

$$\dot{\theta}_i(t) > -T(t, t_m) \left(\tau_i + \rho_i/\gamma_i\right) \theta_i(t).$$

Since $T(t, t_m) = \frac{d}{dt}\zeta(t, \tau)$, integrating both sides yields:

$$\theta_i(t) > \theta_i(0) \cdot \exp\left(-\zeta(t, \tau)\left(\tau_i + \frac{\rho_i}{\gamma_i}\right)\right) > 0. \tag{31}$$

Moreover, according to the triggering rule, $e_i(t) = 0$ at each triggering instant, whereas $\theta_i(t) > 0$ holds. Therefore, $\theta_i(t)$ remains strictly positive for all $t \geq 0$. □

Theorem 1. *Under Assumptions 1–3, the distributed algorithm* (26) *under the DET condition* (27) *ensures the following:*

1) ***Practical PDT Convergence****: The system states globally converge to the optimal solution* $P^*(t)$ *of the TV RMP* (23) *within a PDT* t_m*, i.e.,*

$$\begin{cases} \lim\limits_{t \to t_m^+} \|P(t) - P^*(t)\| \leq \nu, \\ \|P(t) - P^*(t)\| \leq \nu, \quad \forall t > t_m, \\ \lim\limits_{t \to \infty} \|P(t) - P^*(t)\| = 0, \end{cases}$$

where $\nu > 0$ *is a prescribed accuracy parameter.*

2) ***Zeno-Free Behavior****: All inter-event intervals are lower bounded by a strictly positive constant, i.e.,*

$$t_{k+1}^i - t_k^i \geq \sigma/(1+\sigma)\sqrt{B_i^1/B_i^2} > 0,$$

where σ*,* B_i^1*, and* B_i^2 *are positive constants.*

Proof. The proof is divided into two Steps.

Step 1: Practical PDT Convergence.

Define $\tilde{P} = P - P^*$, $\tilde{w} = w - w^*$, $\tilde{\xi} = \xi - \xi^*$ and $\tilde{z} = z - z^*$. Combining (29) and (30), the following error system is obtained

$$\begin{cases} \dot{\tilde{P}} = -T(t, t_m)\left[k_1(\tilde{g} - \tilde{w} - e_w) + \tilde{h} - \tilde{z} - e_z\right], \\ \dot{\tilde{w}} = -T(t, t_m)\left[L(\tilde{w} + e_w) + \tilde{\xi} + e_\xi + k_2(\tilde{P} + e_P)\right], \\ \dot{\tilde{z}} = T(t, t_m)\left[\tilde{h} - \tilde{z} - e_z\right], \\ \dot{\tilde{\xi}} = T(t, t_m) L(\tilde{w} + e_w), \end{cases} \tag{32}$$

where $\tilde{g} = \nabla_P J(P, t) - \nabla_P J(P^*, t)$, and $\tilde{h} = \partial \nabla_P J(P, t)/\partial t - \partial \nabla_P J(P^*, t)/\partial t$. The error vectors $e_P, e_w, e_z, e_\xi \in \mathbb{R}^N$ are defined as in Section IV.

Consider the composite Lyapunov function:

$$V = V_1 + V_2,$$

where $V_1 = \left(\|\tilde{P}\|^2 + \|\tilde{w}\|^2 + \|\tilde{z}\|^2 + \|\tilde{\xi}\|_Q^2\right)/2 + m\|\tilde{w} + \tilde{\xi}\|^2$, with $0 < m < \lambda_2/24$; $V_2 = l\sum_{i=1}^{N} \theta_i(t)$, $\|\tilde{\xi}\|_Q^2 = \tilde{\xi}^T Q \tilde{\xi}$, and $Q = D^T \tilde{H} D$, where D is the orthogonal matrix in the spectral decomposition $L = D^T H D$, and $\tilde{H} = \text{diag}(1, 1/\lambda_2(L), \ldots, 1/\lambda_N(L))$.

The time derivative of V_1 along system (32) is:

$$\begin{aligned} \dot{V}_1 = T(t, t_m)\big(& -k_1 \tilde{P}^T \tilde{g} + k_1 \tilde{P}^T e_w - \tilde{P}^T \tilde{h} + \tilde{P}^T \tilde{z} \\ & + \tilde{P}^T e_z - \tilde{w}^T L \tilde{w} - \tilde{w}^T L e_w - \tilde{w}^T \tilde{\xi} - \tilde{w}^T e_\xi \\ & - k_2 \tilde{w}^T e_P + \tilde{z}^T \tilde{h} - \|\tilde{z}\|^2 - \tilde{z}^T e_z + \tilde{\xi}^T Q L \tilde{w} \\ & + \tilde{\xi}^T Q L e_w - 2m(\tilde{w}^T \tilde{\xi} + \tilde{w}^T e_\xi + \tilde{w}^T e_P \\ & + \|\tilde{\xi}\|^2 + \tilde{\xi}^T e_\xi + \tilde{\xi}^T \tilde{P} + \tilde{\xi}^T e_P).\big) \end{aligned} \tag{33}$$

Using spectral properties of L, we observe that:

$$-\tilde{w}^T\tilde{\xi} = -\tilde{w}^T D^T D\tilde{\xi}, \quad \tilde{\xi}^T QL\tilde{w} = \tilde{\xi}^T D^T D\tilde{w}. \tag{34}$$

Next, applying Young's inequality and eigenvalue bounds, the following estimates hold:

$$\begin{aligned}
&-\tilde{w}^T L\tilde{w} \le -\lambda_2\|\tilde{w}\|^2, -\tilde{w}^T e_\xi \le \lambda_2\|\tilde{w}\|^2/4 + \|e_\xi\|^2/\lambda_2\\
&-\tilde{w}^T L e_w \le \lambda_2\|\tilde{w}\|^2/4 + \lambda_{\max}^2\|e_w\|^2/\lambda_2\\
&-k_2\tilde{w}^T e_P \le \lambda_2\|\tilde{w}\|^2/4 + k_2^2\|e_P\|^2/\lambda_2\\
&-2m\tilde{w}^T\tilde{\xi} \le 4m\|\tilde{w}\|^2 + m\|\tilde{\xi}\|^2/4\\
&-2m\tilde{w}^T e_\xi \le m\|\tilde{w}\|^2 + m\|e_\xi\|^2\\
&-2m\tilde{w}^T e_P \le m\|\tilde{w}\|^2 + m\|e_P\|^2\\
&-\tilde{z}^T e_z \le \|\tilde{z}\|^2/4 + \|e_z\|^2, \tilde{z}^T\tilde{h} \le \|\tilde{z}\|^2/4 + \bar{l}\|\tilde{P}\|^2.
\end{aligned} \tag{35}$$

where $\bar{l} = \max_i\{l_i\}$ is the uniform Lipschitz constant for $\partial_t\nabla J_i$. For all terms containing $\tilde{P}$, one has

$$\begin{aligned}
&-k_1\tilde{P}^T\tilde{g} = -k_1\tilde{P}^T(\nabla_P J - \nabla_P J^*) \le -k_1\underline{c}\|\tilde{P}\|^2\\
&-\tilde{P}^T\tilde{h} = -\tilde{P}^T(\partial\nabla_P J/\partial t - \partial\nabla_P J^*/\partial t) \le \bar{l}\|\tilde{P}\|^2\\
&\tilde{P}^T e_z \le \|\tilde{P}\|^2 + \|e_z\|^2/4,\ \tilde{P}^T\tilde{z} \le \|\tilde{z}\|^2/4 + \|\tilde{P}\|^2\\
&\tilde{P}^T e_w \le k_1\underline{c}\|\tilde{P}\|^2/2 + k_1\|e_w\|^2/(2\underline{c})\\
&-2m\tilde{\xi}^T\tilde{P} \le m\|\tilde{\xi}\|^2/4 + 4m\|\tilde{P}\|^2.
\end{aligned} \tag{36}$$

Where $\underline{c} = \min_i\{c_i\}$. For all terms containing $\tilde{z}$, we have

$$-\tilde{z}^T e_z = \|\tilde{z}\|^2/4 + \|e_z\|^2, \tilde{z}^T\tilde{h} \le \|\tilde{z}\|^2/4 + \bar{l}\|\tilde{P}\|^2. \tag{37}$$

For the remaining terms in (33), one can obtain

$$\begin{aligned}
&\tilde{\xi}^T QLe_w \le m\|\tilde{\xi}\|^2/4 + \lambda_{\max}^2\|e_w\|^2/(m\lambda_2^2)\\
&-2m\tilde{\xi}^T e_\xi \le m2\|\tilde{\xi}\|^2/2 + 2me_\xi\|^2\\
&-2m\tilde{\xi}^T e_P \le m\|\tilde{\xi}\|^2/4 + 4m\|e_P\|^2.
\end{aligned} \tag{38}$$

Substituting (34)– (38) into (33) yields

$$\begin{aligned}
\dot{V}_1 \le& T(t,t_m)(-s_1\|\tilde{w}\|^2 - s_2\|\tilde{P}\|^2 - s_3\|\tilde{z}\|^2 - s_4\|\tilde{\xi}\|^2 +\\
&+ l\sum_{i=1}^N(e_{Pi}^2 + e_{wi}^2 + e_{zi}^2 + e_{\xi i}^2)).
\end{aligned}$$

Where $s_1 = \lambda_2/4 - 6m$, $s_2 = k_1\underline{c}/2 - 4m - 2\bar{l}$, $s_3 = 3/4$, $s_4 = m/2$, $l = \max\{\lambda_{\max}^2/\lambda_2 + k_1/(2\underline{c}) + \lambda_{\max}^2/(m\lambda_2^2), k_2^2/\lambda_2 + 5m, 5/4, 1/\lambda_2 + 3m\}$.

Next, taking the derivative of V_2 along the trajectory of system (32), we obtain

$$\dot{V}_2 = l\sum_{i=1}^N\dot{\theta}_i = lT(t,t_m)\sum_{i=1}^N(-\tau_i\theta_i - \rho_i e_i). \tag{39}$$

Combining with the estimate on $\dot{V}_1$ and invoking the DET triggering condition (27), we have:

$$\begin{aligned}
\dot{V} &= \dot{V}_1 + \dot{V}_2\\
&\le T(t,t_m)\Big(-s_1\|\tilde{w}\|^2 - s_2\|\tilde{P}\|^2 - s_3\|\tilde{z}\|^2\\
&\quad - s_4\|\tilde{\xi}\|^2 - l\sum_{i=1}^N\tau_i\theta_i + l\sum_{i=1}^N(1-\rho_i)e_i\Big).
\end{aligned} \tag{40}$$

Applying the triggering condition $\gamma_i e_i(t) < \theta_i(t)$ during inter-event intervals yields:

$$\begin{aligned}
\dot{V} \le& T(t,t_m)\sum_{i=1}^N\Big(-s_1\|\tilde{w}\|^2 - s_2\|\tilde{P}\|^2 - s_3\|\tilde{z}\|^2\\
&- s_4\|\tilde{\xi}\|^2 - l\left(\tau_i - (1-\rho_i)/\gamma_i\right)\theta_i\Big).
\end{aligned} \tag{41}$$

By virtue of $\rho_i \in (0,1)$ and $\gamma_i > (1-\rho_i)/\tau_i$, $\tau_i - (1-\rho_i)/\gamma_i > 0$ holds. Let $m_1 = \min\{\gamma_i > (1-\rho_i)/\tau_i,\ \forall i = 1,...,N$, we further obain

$$\dot{V} \le -m_2 T(t,t_m)(\tilde{w}^T\tilde{w} + \tilde{P}^T\tilde{P} + \tilde{z}^T\tilde{z} + \tilde{\xi}^T\tilde{\xi} + l\sum_{i=1}^N\theta_i),$$

where $m_2 = \min\{s_1, s_2, s_3, m_1\}$. According to the expression of V, one can get that $V \le m_3(\tilde{w}^T\tilde{w} + \tilde{P}^T\tilde{P} + \tilde{z}^T\tilde{z} + \tilde{\xi}^T\tilde{\xi} + l\sum_{i=1}^N\theta_i)$, with $m_3 = \max\{1, 1/2 + 2m, 1/(2\lambda_2) + 2m\}$. Therefore, we have

$$\dot{V} \le -(m_2/m_3)T(t,t_m)V. \tag{42}$$

According to (2) and (42), the following equation can be obtained:

$$\|P - P^*\|^2 = \|\tilde{P}(t)\|^2 \le V(t) \le V(0)e^{-(m_2/m_3)(\zeta(t)-\zeta(0))}, \tag{43}$$

which implies that

$$\lim_{t\to t_{m+}}\|P - P^*\| \le \sqrt{V(0)e^{-(m_2/m_3)(\zeta(t_{m+})-\zeta(0))}}. \tag{44}$$

Next, let $\nu = \sqrt{V(0)e^{-(m_2/m_3)(\zeta(t_{m+})-\zeta(0))}}$, it follows that $\lim_{t\to t_{m+}}\|P - P^*\| \le \nu$, this implies that (1) in Definition 1 satisfies. Together with (43), (44) and the expression of $\zeta(t)$, for any $\tilde{t} > t_m$, one gets

$$\|P(\tilde{t}) - P^*\|^2 \le V(0)e^{-(m_2/m_3)(\zeta(t_{m+})-\zeta(0))} = \nu^2, \tag{45}$$

That is $\|P(\tilde{t}) - P^*\| \le \nu$, $\forall\tilde{t} > t_m$, this indicates that (2) in Definition 1 holds. Moreover, it is straightforward to derive that $\lim_{t\to+\infty}\|P - P^*\| = 0$. This demonstrates that, (3) in Definition 1 holds.

Step 2: Zeno-Free Behavior.

For any $t \in [t_k^i, t_{k+1}^i)$, the sampled variables $\hat{P}_i(t), \hat{w}_i(t), \hat{z}_i(t), \hat{\xi}_i(t)$ remain constant. Thus, the upper right Dini derivatives of the corresponding error terms satisfy: $D^+e_{Pi} = -\dot{P}_i$, $D^+e_{wi} = -\dot{w}_i$, $D^+e_{zi} = -\dot{z}_i$, $D^+e_{\xi i} = -\dot{\xi}_i$. Taking into account $e_{Pi}(t_k^i) = e_{wi}(t_k^i) = e_{zi}(t_k^i) = e_{\xi i}(t_k^i) = 0$, we have $e_{Pi} = -\int_{t_k^i}^t\dot{P}_i(t)dt$, $e_{wi} = -\int_{t_k^i}^t\dot{w}_i(t)dt$, $e_{zi} = -\int_{t_k^i}^t\dot{z}_i(t)dt$, $e_{\xi i} = -\int_{t_k^i}^t\dot{\xi}_i(t)dt$.

By view of the definition of $T(t,t_m)$ in [39], it implies $T(t,t_m) \le \sigma/(1+\sigma)$ with small enough positive constant σ, $\forall t \in [t_k^i, t_{k+1}^i)$. Let $B_{P_i} = \max_t\{|P_i|\}$, $B_{w_i} = \max_t\{|w_i|\}$, $B_{z_i} = \max_t\{|z_i|\}$, $B_{\xi_i} = \max\{|\xi_i|\}$, $B_{J_i} = \max_t\{|\nabla_P J_i|\}$, and $B_{Jt_i} = \max_t\{|\partial\nabla_P J_i/\partial t|\}$ for all $t \in [t_k^i, t_{k+1}^i)$. Next, by system (26), the state derivatives are bounded by:

$$\begin{aligned}
&\|\dot{P}_i\| \le (1+\sigma)(k_1B_{J_i} + B_{Jt_i} + k_1B_{w_i} + B_{z_i})/\sigma\\
&\|\dot{w}_i\| \le (1+\sigma)(2B_{w_i}l_{ii} + B_{\xi_i} + k_2d_i + k_2B_{P_i})/\sigma\\
&\|\dot{z}_i\| \le (1+\sigma)(B_{Jt_i} + B_{z_i})/\sigma\\
&\|\dot{\xi}_i\| \le (1+\sigma)(2B_{w_i}l_{ii})/\sigma.
\end{aligned} \tag{46}$$

Combining these bounds, the error $e_i(t)$ over $t \in [t_k^i, t_{k+1}^i)$ satisfies:

$$e_i(t) \leq ((1+\sigma)/\sigma)^2 (t - t_k^i)^2 B_1^i, \tag{47}$$

where $B_1^i = (k_1 B_{J_i} + B_{Jt_i} + k_1 B_{w_i} + B_{z_i})^2 + (2B_{w_i} l_{ii} + B_{\xi_i} + k_2 d_i + k_2 B_{P_i})^2 + (B_{Jt_i} + B_{z_i})^2 + (2B_{w_i} l_{ii})^2$. We further obtain that

$$e_i(t_{k+1}^i) \leq ((1+\sigma)/\sigma)^2 (t_{k+1}^i - t_k^i)^2 B_1^i. \tag{48}$$

At the triggering instant $t = t_{k+1}^i$, the condition $\gamma_i e_i(t_{k+1}^i) = \theta_i(t_{k+1}^i)$ holds. In accordance with (31), one has

$$e_i(t_{k+1}^i) \geq \theta_i(0) \exp(\zeta(t_{k+1}^i, \tau)(\tau_i + \rho_i/\gamma_i)). \tag{49}$$

Combining (48) and (49), yields

$$t_{k+1}^i - t_k^i \geq (1+\sigma)/\sigma \sqrt{B_2^i / B_1^i}.$$

Where $B_2^i = \theta_i(0) \exp(\zeta(t_{k+1}^i, \tau)(\tau_i + \rho_i/\gamma_i))$. The right-hand side is strictly positive, ensuring a uniform minimum time interval between events and excluding Zeno behavior. □

Remark 7. *Theorem 1 and Lemma 4 jointly establish that the proposed distributed algorithm* (26) *guarantees PDT convergence to the optimal solution of the barrier-based problem* (25)*, while strictly maintaining both equality and inequality constraints throughout its execution. Moreover, since the solution of* (25) *asymptotically converges to that of the original constrained problem* (23)*, the algorithm ensures that a strictly feasible, near-optimal decision is achieved within a user-defined horizon and refined over time. This dual property of fast feasibility and long-term optimality makes the method well-suited for real-time and safety-critical applications.*

Remark 8. *The proposed DET algorithm can be extended to discrete-time settings using a forward Euler discretization with fixed step size κ, leading to the following update scheme:*

$$\begin{cases} P_i(k+1) = P_i(k) - \kappa T(t_k, t_m)(k_1 \nabla_P J_i(P_i(k)) \\ \qquad + \partial \nabla_P J_i(P_i(k))/\partial t - k_1 w_i(k) - z_i(k)) \\ w_i(k+1) = w_i(k) - \kappa T(t_k, t_m)(\sum_{j \in N_i} a_{ij}(w_i(k) \\ \qquad - w_j(k)) + \xi_i(k) - k_2 d_i(k) + k_2 P_i(k)) \\ z_i(k+1) = z_i(k) + \kappa T(t_k, t_m)(\partial/\nabla_P J_i(P_i(k))/\partial t - z_i(k)) \\ \xi_i(k+1) = \xi_i(k) + \kappa T(t_k, t_m) \sum_{j \in N_i} a_{ij}(w_i(k) - w_j(k)). \end{cases}$$

Under similar conditions to those in Theorem 1, convergence of the discrete-time scheme can be established. However, extending PDT guarantees to discrete-time domains poses new challenges, which will be addressed in future work.

Remark 9. *This work considers a standard DET framework under the assumption of a secure communication environment. However, in practical cyber-physical systems such as MGs, event-triggered strategies may become vulnerable to adversarial attacks, such as data falsification or denial-of-service, which can manipulate triggering behavior or disrupt information exchange. Therefore, developing attack-resilient event-triggered distributed control mechanisms represents an important and challenging direction for future research.*

V. Simulation Results

This section evaluates the effectiveness of the proposed distributed DET-PDT optimization strategy in addressing TV constraints, reducing communication overhead, and ensuring scalability in MG operation. A six-agent MG system is considered, consisting of five representative device units and a grid interface. The physical and communication topologies are illustrated in Fig. 2 and Fig. 3, respectively. To reflect realistic dynamics, each agent's objective is modeled as a time-varying quadratic function $\tilde{W}_i = \delta_i(t) P_i^2 + \eta_i(t) P_i + \vartheta_i(t)$. In addition, the TV critical parameter configurations of the objective functions for each unit are detailed in Table II, where $w_1 = 0.1\pi/10$, and $w_2 = 8\pi/75$. The DET parameters are specified as follows: $\gamma = [3, 5, 1, 2, 5, 1.5]$, $\tau = [0.02, 0.01, 0.02, 0.01, 0.02, 0.01]$, and $\alpha = [20, 15, 10, 10, 8, 8]$, for agents $i = 1$ to 6, respectively. The parameter ρ_i is uniformly set to 0.1 for all agents. These parameters are selected to ensure sufficient triggering sensitivity near the predefined time t_m, while maintaining a reasonable balance between communication load and convergence precision.

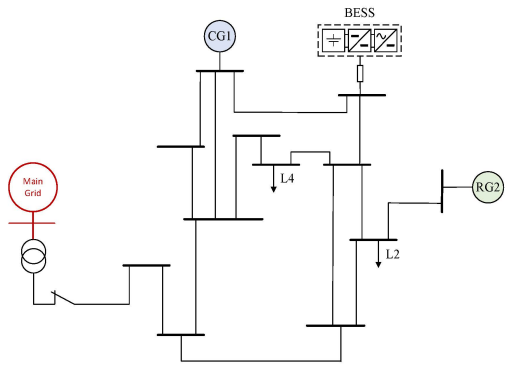

Fig. 2. Schematic of the MG system.

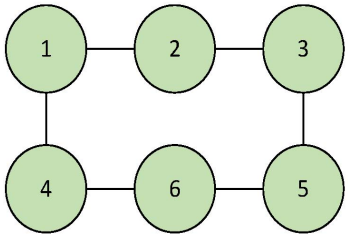

Fig. 3. Communication topology among the six agents.

This setting enables the proposed DET-PDT algorithm to be evaluated under realistic operational conditions. The results presented in the subsequent subsections demonstrate not only the algorithm's effectiveness in ensuring real-time convergence

TABLE II
TV SWF PARAMETERS AND INEQUALITY CONSTRAINTS

Unit	$\delta_i(t)$	$\eta_i(t)$	$\vartheta_i(t)$
CDG	$1.3(2+0.1sin(w_1t+\frac{\pi}{2}))$	$-1+0.5cosw_2t$	$0.5+0.02t$
REG	$3.8(1+sin(w_1t+\frac{\pi}{4}))$	$0.8+0.4cosw_2t$	$0.4+0.01t$
ESS	$2.4(1.2+sin(w_1t+\frac{\pi}{5}))$	$-0.5+0.3cosw_2t$	$0.6+0.03t$
Load 1	$3.2(1+sin(w_1t+\frac{2\pi}{3}))$	$-1.8+0.6cosw_2t$	$0.3+0.02t$
Load 2	$0.8(1+sin(w_1t+\frac{2\pi}{3}))$	$-0.6+0.45cosw_2t$	$0.7+0.01t$
GI	$2+0.1sin(w_1t+\frac{\pi}{12})$	$0.5+0.3cosw_2t$	$0.5+0.03t$
	$d_i(t)$	P_i^{min}	P_i^{max}
CDG	$5+1.2sin(w_2t+\frac{\pi}{2})$	0	13
REG	$4+1.5sin(w_2t+\frac{\pi}{6})$	0	7
ESS	$6+2.5sin(w_2t+\frac{\pi}{4})$	-10	10
Load 1	$7+3sin(w_2t+\frac{\pi}{3})$	-1.8	5
Load 2	$6+2sin(w_2t+\frac{\pi}{2})$	5	20
GI	$8+2sin(w_2t+\frac{\pi}{2})$	-10	20

and TV constraint satisfaction, but also its ability to significantly reduce communication overhead.

Remark 10. *It is worth pointing out that the selection of the DET parameters α_i, τ_i, and the PDT t_m are tuned based on the trade-off between communication frequency and convergence precision. Specifically, α_i sets the initial value of the triggering threshold, where larger values reduce early triggering and smaller ones increase sensitivity. The parameter τ_i controls the decay rate of the threshold function. A larger τ_i results in faster decay, which enhances triggering sensitivity as the system approaches t_m, helping to improve convergence accuracy near the predefined deadline. The PDT t_m represents the user-specified convergence horizon and can be selected based on the system's desired response time. A smaller t_m leads to faster convergence but may require more frequent triggering and larger control effort. In practice, these parameters are jointly tuned to balance convergence speed, communication load, and control performance.*

A. *Effectiveness test*

This case study demonstrates the PDT convergence behavior and real-time optimization capability of the proposed DET-PDT strategy in grid-connected MG operation. The time-based function $T(t,t_m)$ is initialized at $t=0\,\mathrm{s}$ with a convergence deadline $t_m=5\,\mathrm{s}$, given by:

$$T(t,t_m)=\begin{cases}\frac{1+10\left(\frac{60}{5^6}t^5-\frac{120}{5^5}t^4+\frac{60}{5^4}t^3\right)}{1-10\left(\frac{10}{5^6}t^6-\frac{24}{5^5}t^5+\frac{15}{5^4}t^4\right)+10}, & 0\le t\le t_m,\\ 1, & t>t_m.\end{cases}$$

Fig. 4(a)–(d) illustrate the system's critical operational trajectories under the proposed strategy. Fig. 4(a) demonstrates that the total power supply tracks the demand closely, even under significant load fluctuations, confirming the algorithm's effectiveness in real-time demand-following and dynamic adaptability. Fig. 4(b) shows the DET instants. it can be observed that communication is only activated when the critical state deviation exceeds the preset threshold, which verifies that the algorithm achieves efficient collaboration by reducing redundant communication, greatly reducing the communication burden. The marginal utility function trajectories of all participating units in the MG rapidly achieve consensus

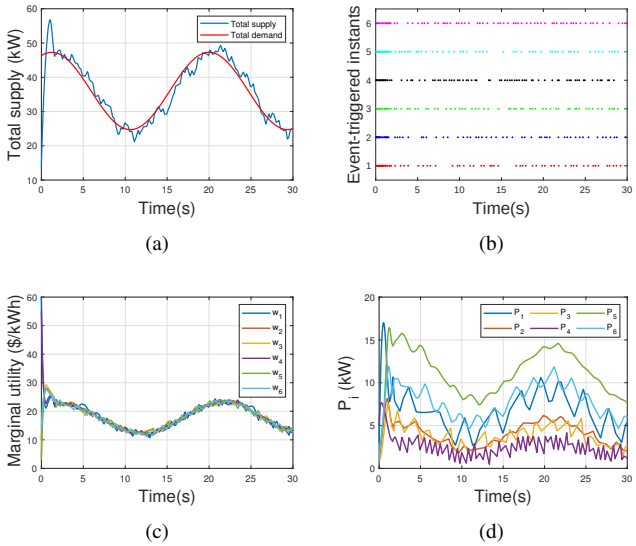

Fig. 4. (a) Real-time demand-supply synchronization; (b) Distributed DET triggering instants; (c) Marginal utility trajectories (w); (d) Power evolution of P_1–P_6.

within the PDT $t_m=5s$ in Fig. 4(c). The consistency of the derivatives of objective function confirms the strict satisfaction of Pareto optimality in RMP. Fig. 4(d) displays the optimal dynamic evolution of the participating units.

To further assess generality, we evaluated the algorithm under static conditions with time-invariant coefficients, as detailed in Table III. In this case, the predefined time was set to $t_m=15s$. The results in Fig. 5 show that the proposed DET-PDT strategy remains highly effective. Specifically, it achieves lower communication overhead, stable supply-demand synchronization, and rapid marginal utility alignment.

These findings confirm that the algorithm not only adapts to highly dynamic TV environments but also maintains strong performance in static resource management scenarios, demonstrating broad applicability and robustness.

TABLE III
STATIC SWF PARAMETERS AND INEQUALITY CONSTRAINTS

Unit	δ_i	η_i	ϑ_i	d_i	$P_i^{\min}$	$P_i^{\max}$
CDG	2	1	0	5	0	13
REG	3	1	2	10	0	5
ESS	1	2	-1	4	-5	5
Load 1	3	3	6	2.5	2	10
Load 2	2	1	7	7	5	13
GI	1	1	3	3	0	20

To evaluate the influence of the PDT t_m, we compare the marginal utility convergence under different t_m settings. As illustrated in Fig. 6 and Fig. 5(c), since t_m defines the upper bound of the convergence time, smaller values lead to faster convergence. However, due to the design of the DET condition in Eq. (28), a smaller t_m also results in a more sensitive triggering threshold, thereby increasing the triggering frequency. Specifically, the total number of triggering events rises from 320 ($t_m=15\,\mathrm{s}$) to 407 ($t_m=10\,\mathrm{s}$) and 732

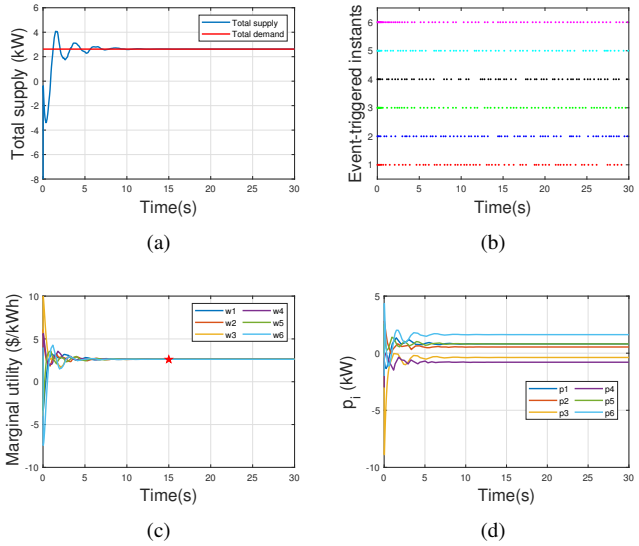

Fig. 5. (a) Demand-supply match; (b) Event-triggered communication; (c) Marginal utility convergence with $t_m = 15s$; (d) Power trajectories under static setup.

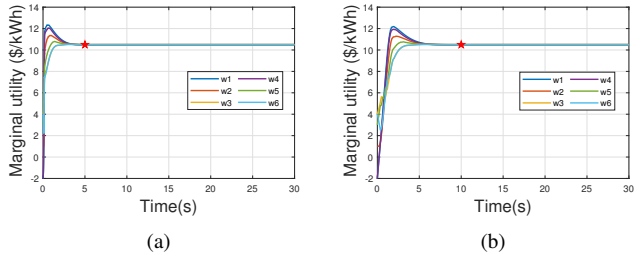

Fig. 6. (a) Marginal utility convergence with $t_m = 5s$; (b) Marginal utility convergence with $t_m = 10s$.

($t_m = 5$ s). Therefore, the selection of t_m requires a careful balance between convergence speed and triggering cost.

B. Plug-and-play (PnP) Capability Test

To assess the proposed algorithm's resilience to structural changes in MG topology, we conduct a PnP test involving the disconnection and reconnection of agent 6 (the main grid). During disconnection, the agent's state variables (P_i, w_i, z_i and ξ_i) are set to zero to remove its effect on system dynamics, while the communication topology remains unchanged. This simplified treatment reflects practical scenarios where the main grid is temporarily unavailable due to faults, islanding protection, or scheduled maintenance, while the communication infrastructure remains operational. Specifically, agent 6 is disconnected at $t = 10$ s and reconnected at $t = 20$ s. In both events, the TBG function $T(t, t_m)$ is reset with a new convergence deadline $t_m = 2s$.

As shown in Fig. 7(a), a marked increase in event-triggering activity is observed immediately after both disconnection and reconnection, reflecting the system's rapid response to topology variation. Fig. 7(b) illustrates the total supply (blue curve) dynamically tracks the total demand (red curve) over time. Although short-term oscillations are observed in the

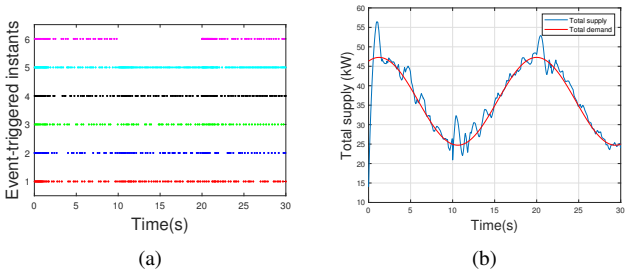

Fig. 7. (a) Distributed DET communication sequence under PnP capability test; (b) Real-time demand-supply synchronization under PnP capability test.

supply curve, particularly during transition phases the overall trend of supply closely aligns with the demand trajectory. When agent 6 is disconnected at $t = 10$ s, the total supply drops sharply due to the loss of grid support. However, the remaining units promptly adjust their outputs, enabling the system to continue tracking the total demand with minimal delay. Similarly, upon reconnection at $t = 20$ s, the total supply surges, and the system swiftly rebalances to maintain demand-supply alignment. This demonstrates the algorithm's strong adaptability and coordination under structural changes. Although the proposed method is demonstrated on a system with 6 agents, its performance and computational scalability for large-scale multi-agent systems require further investigation.

C. Comparative experiment

To further evaluate communication performance, this section conducts a comparative study with existing event-triggered strategies. Fig. 8 compares the event-triggering behaviors of three strategies applied to the same TV RMP: (i) the DET approach from [46], (ii) the static event-triggered strategy in [15], and (iii) the proposed DET-PDT method.

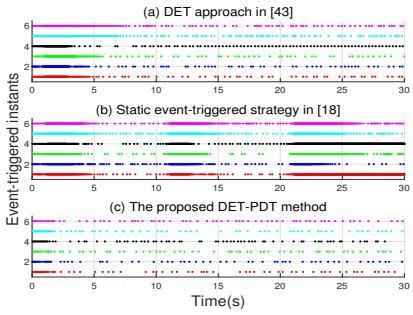

Fig. 8. Comparison of event-triggered strategies from [46], [15], and this paper.

As shown, the benchmark methods in [46] and [15] exhibit frequent and clustered triggering, especially during the initial period, indicating limited ability to suppress redundant communication. In contrast, the proposed DET-PDT strategy achieves more uniformly distributed and significantly fewer triggers across agents and time. This improvement results from the adaptive threshold mechanism $\theta_i(t)$ (see Remark 4),

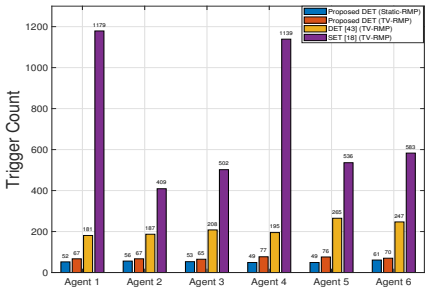

Fig. 9. Trigger counts per agent under different strategies.

which effectively balances responsiveness and communication efficiency.

Fig. 9 compares the total number of triggering events for six agents under different strategies: (i) the proposed DET-PDT for a static RMP, (ii) the proposed DET-PDT applied to a TV RMP, (iii) the DET method in [46] under the same TV RMP as in (ii), and (iv) the SET method in [15], also tested under the same TV RMP as in (ii). For the same time-varying resource management problem, the proposed DET-PDT method yields only 422 triggers, reducing communication by 67.1% compared to the DET strategy in [46] (1283 triggers) and by 90.3% relative to the static method in [15] (4348 triggers). Moreover, when applied to a static scenario, the number of triggers further drops to 320, highlighting the method's adaptability and communication efficiency in both dynamic and static settings.

VI. Conclusion

In this paper, the TV RMP with TV demand constraints in MG has been studied by using an MAS framework. To address this challenge, a novel distributed DET algorithm has been developed based on a TBG function, which features PDT convergence, initialization-free operation, and a reduced communication burden. Furthermore, the DET mechanism has been specially designed to further reduce the communication overhead in the TV RMP. Finally, the proposed approach has been rigorously validated through simulations, including effectiveness testing, PnP capability evaluation and the comparative experiment. In the future, the integration of adaptive event-triggered strategies, attack detection mechanisms, and scalability to large-scale systems will be further explored.

References

[1] F. Mostafa, W. John, A. Patricio, et al., Microgrid stability definitions, analysis, and examples, IEEE Transactions on Power Systems 35 (1) (2020) 13–29.

[2] E. Espina, J. Llanos, C. Burgos-mellado, et al., Distributed control strategies for microgrids: An overview, IEEE Access 8 (2020) 193412–193448.

[3] R. de Azevedo, M. Cintuglu, T. Ma, et al., Multiagent-based optimal microgrid control using fully distributed diffusion strategy, IEEE Transactions on smart grid 8 (4) (2017) 1997–2008.

[4] M. Abid, H. Apon, S. Hossain, et al., Distributed event-triggering algorithm with uncoordinated step sizes for economic dispatch problem over unbalanced directed network, International Journal of Electrical Power and Energy Systems 353 (2024) 122029.

[5] Q. Liu, X. Le, K. Li, A distributed optimization algorithm based on multiagent network for economic dispatch with region partitioning, IEEE Transactions on Cybernetics 51 (5) (2019) 2466–2475.

[6] K. Wu, Q. Li, Z. Chen, et al., Distributed optimization method with weighted gradients for economic dispatch problem of multi-microgrid systems, Energy 222 (2021) 119898.

[7] P. Feng, X. He., Mixed neurodynamic optimization for the operation of multiple energy systems considering economic and environmental aspects, Energy 232 (2021) 120965.

[8] B. Wang, S. Sun, W. Ren, Distributed time-varying quadratic optimal resource allocation subject to non-identical time-varying hessians with application to multiquadrotor hose transportation, IEEE Transactions on Systems, Man, and Cybernetics: Systems 52 (10) (2022) 6109–6119.

[9] B. Huang, Y. Zou, F. Chen, et al., Distributed time-varying economic dispatch via a prediction-correction method, IEEE Transactions on Circuits and Systems I: Regular Papers 69 (10) (2022) 4215–4224.

[10] W. Zhu, Q. Wang, Distributed finite-time optimization of multi-agent systems with time-varying cost functions under digraphs, IEEE Transactions on Network Science and Engineering 11 (1) (2024) 556–565.

[11] B. Wang, S. Sun, W. Ren, Distributed continuous-time algorithms for optimal resource allocation with time-varying quadratic cost functions, IEEE Transactions on Control of Network Systems 7 (4) (2020) 1974–1984.

[12] G. Seyboth, D. Dimarogonas, K. Johansson, Event-based broadcasting for multi-agent average consensus, Automatica 49 (1) (2013) 245–252.

[13] P. Tabuada, Event-triggered real-time scheduling of stabilizing control tasks, IEEE Transactions on Automatic Control 52 (2007) 1680–1685.

[14] X. Shangguan, Y. He, C. Zhang, et al., Load frequency control of time-delayed power system based on event-triggered communication scheme, Applied Energy 308 (2022) 118294.

[15] Y. Li, H. Zhang, X. Liang, et al., Event-triggered-based distributed cooperative energy management for multienergy systems, IEEE Transactions on Industrial Informatics 15 (4) (2019) 2008–2022.

[16] L. Ji, M. Shen, S. Yang, et al., A distributed event-triggered algorithm for constrained economic dispatch problem via virtual communication, International Journal of Electrical Power and Energy Systems 145 (2023) 108601.

[17] X. Bu, R. Luo., Attitude control with discrete-time prescribed performance for seeker stabilized platform via event-triggered neural approximation, IEEE Transactions on Industrial Informatics 21 (2) (2025) 1853–1861.

[18] D. Zhou, Dynamic event-triggered distributed observer for linear systems, ISA Transactions 137 (2023) 87–97.

[19] F. Yang, J. Liu, X. Guan, Distributed fixed-time optimal energy management for microgrids based on a dynamic event-triggered mechanism, IEEE/CAA Journal of Automatica Sinica 11 (12) (2024) 2396–2407.

[20] B. Chen, J. Yang, W. Lu, et al., A distributed algorithm with dynamic event-triggered mechanism for resource allocation problems, Cluster Computing 28 (17) (2025). doi:org/10.1007/s10586-024-04693-z.

[21] Z. Dong, S. Mao, M. Perc, et al., A distributed dynamic event-triggered algorithm with linear convergence rate for the economic dispatch problem, IEEE Transactions on Network Science and Engineering 10 (1) (2022) 500–513.

[22] Z. Guo, G. Chen, Distributed dynamic event-triggered and practical predefined-time resource allocation in cyber–physical systems, Automatica 142 (2022) 110390.

[23] Y. Xu, Z. Li, Distributed optimal resource management based on the consensus algorithm in a microgrid, IEEE Transactions on Industrial Electronics 62 (4) (2015) 2584–2592.

[24] Q. Li, Y. Liao, K. Wu, et al., Parallel and distributed optimization method with constraint decomposition for energy management of microgrids, IEEE Transactions on Smart Grid 12 (6) (2021) 4627–4640.

[25] Y. Li, P. Dong, M. Liu, et al., A distributed coordination control based on finite-time consensus algorithm for a cluster of dc microgrids, IEEE Transactions on Power Systems 34 (3) (2019) 2205–2215.

[26] M. Zaery, P. Wang, R. Huang, et al., Distributed economic dispatch for islanded dc microgrids based on finite-time consensus protocol, IEEE Access 8 (2020) 192457–192468.

[27] T. Zhao, Z. Ding, Distributed finite-time optimal resource management for microgrids based on multi-agent framework, IEEE Transactions on Industrial Electronics 65 (8) (2018) 6571–6580.

[28] X. Liu, X. He, C. Li, et al., Deep learning and projection neural network with finite-time convergence for energy management of multi-energy system, IEEE Transactions on Smart Grid 16 (3) (2025) 2156–2168.

[29] X. Bu, R. Luo, H. Lei., Chattering-avoidance discrete-time fuzzy control with finite-time preselected qualities, IEEE Transactions on Fuzzy System 33 (3) (2025) 997–1008.

[30] H. Hong, W. Yu, G. Jiang, et al., Fixed-time algorithms for time-varying convex optimization, IEEE Transactions on Circuits and System-II: Express Beiefs 70 (2) (2023) 616–620.

[31] G. Chen, Q. Yang, Y. Song, et al., Fixed-time projection algorithm for distributed constrained optimization on time-varying digraphs, IEEE Transactions on Automatic Control 67 (1) (2022) 390–397.

[32] L. Liu, G. yang, Distributed fixed-time optimal resource management for microgrids, IEEE Transactions on Automation Science and Engineering 20 (1) (2023) 404–412.

[33] Z. Li, G. Chen, Fixed-time consensus based distributed economic generation control in a smart grid, International Journal of Electrical Power and Energy Systems 134 (2022) 107437.

[34] X. Bu, H. Lei., Fixed-time prescribed performance unknown direction control of discrete-time non-affine systems without nussbaum-type function, IEEE Transactions on Automatic Science and Engineering 21 (4) (2025) 7064–7072.

[35] Z. Guo, G. Chen, Predefined-time distributed optimal allocation of resources: a time-base generator scheme, IEEE Transactions on Systems, Man, and Cybernatics: Systems 52 (1) (2022) 438–447.

[36] A. Kantamneni, L. E. Brown, G. Parker, et al., Survey of multi-agent systems for microgrid control, Engineering Applications of Artificial Intelligence 45 (2015) 192–203.

[37] D. K. Molzahn, F. Dörfler, H. Sandberg, et al., A survey of distributed optimization and control algorithms for electric power systems, IEEE Transactions on Smart Grid 8 (6) (2017) 2941–2962.

[38] Y. Liu, Z. Xia, W. Gui, Multiobjective distributed optimization via a predefined-time multiagent approach, IEEE Transactions on Automatic Control 68 (11) (2023) 6998–7005.

[39] S. Li, X. Nian, Z. Deng, et al., Predefined-time distributed optimization of general linear multi-agent systems, Information Sciences 584 (5) (2021) 111–125.

[40] Y. Pan, L. Ju, S. Yang, et al., A multi-objective robust optimal dispatch and cost allocation model for microgrids-shared hybrid energy storage system considering flexible ramping capacity, Applied Energy 369 (2024) 123565.

[41] M. Amini, M. Nazari, S. Hosseinian., Optimal energy management of battery with high wind energy penetration: A comprehensive linear battery degradation cost model, Sustainable Cities and Society 93 (2023) 104492.

[42] L. Liu, G. Yang, S. Wasly., Distributed predefined-time dual-mode energy management for a microgrid over event-triggered communication, IEEE Transactions on Industrial Informatics 3 (20) (2024) 3295–3305.

[43] S. Sun, J. Xu, W. Ren, Distributed continuous-time qlgorithms for time-varying constrained convex optimization, IEEE Transactions on Automatic Control 68 (7) (2023) 3931–3946.

[44] B. Huang, Y. Zou, Z. Meng, et al., Distributed time-varying convex optimization for a class of nonlinear multi-agent systems, IEEE Transactions on Automatic Control 65 (2) (2020) 801–808.

[45] M. Fazlyab, S. Paternain, V. M. Preciado, et al., Prediction correction interior-point method for time-varying convex optimization, IEEE Transactions on Automatic Control 63 (7) (2018) 1973–1986.

[46] S. Chen, Z. Yu, Distributed predefined-time optimization algorithm: dynamic event-triggered control, IEEE Transactions on Control of Network Systems 11 (1) (2024) 486–497.